SCIENCE CHINA
Information Sciences

• RESEARCH PAPER •

November 2022, Vol. 65 212302:1–212302:18
https://doi.org/10.1007/s11432-021-3438-7

A robust tracking method focusing on target fluctuation and maneuver characteristics

Weiming TIAN[1,3], Linlin FANG[1,3], Rui WANG[1,2,3], Weidong LI[1,2*], Chao ZHOU[1] & Cheng HU[1,2,3]

[1] *Radar Research Lab, School of Information and Electronics, Beijing Institute of Technology, Beijing 100081, China;*
[2] *Advanced Technology Research Institute, Beijing Institute of Technology, Jinan 250300, China;*
[3] *Key Laboratory of Electronic and Information Technology in Satellite Navigation (Beijing Institute of Technology), Ministry of Education, Beijing 100081, China*

Received 16 September 2021/Revised 5 January 2022/Accepted 22 February 2022/Published online 25 October 2022

Abstract Radar is an important tool for aiding in bird strike mitigation as part of overall safety management systems at civilian and military airfields. However, the diverse movement trajectories and irregular echo power fluctuations cause existing multitarget tracking algorithms to face many challenges such as detection uncertainty and maneuver uncertainty. Therefore, this paper proposes a robust tracking method focusing on target fluctuation and maneuver characteristics. Firstly, a tracking information feedback mechanism based on the fluctuation model of bird targets is established, and the measurement set in the predicted gate is reconstructed to solve the problem of track breakages caused by the echo power fluctuation. Secondly, an adaptive parameter filter model is designed to enhance maneuver adaptability. Finally, simulation and experimental data verification show that the proposed method is more adaptive to bird target characteristics and can effectively improve the tracking performance without significantly increasing computation.

Keywords radar, bird targets, echo power fluctuation, maneuver, multitarget tracking

Citation Tian W M, Fang L L, Wang R, et al. A robust tracking method focusing on target fluctuation and maneuver characteristics. Sci China Inf Sci, 2022, 65(11): 212302, https://doi.org/10.1007/s11432-021-3438-7

1 Introduction

Bird strike is a significant threat to flight safety and has caused a number of accidents with human casualties. Statistics indicate that bird-aircraft collisions constitute one of the highest risks to aircraft [1]. In addition, collisions between man-made structures and conveyances and birds are contributing factors, among many others, to the worldwide decline of many avian species [2]. Therefore, the effective prevention of bird strike will bring huge economic and ecological benefits to mankind. Radar, which has a wide detection range and is independent of light and weather, is an established research tool for bird target tracking [3–5]. However, affected by various factors such as electromagnetic frequency, target attitude, and radar observation angle, the echo power of bird targets usually presents with random and irregular fluctuations [6–8], resulting in measurement loss in a short time and track breakages. Moreover, the maneuvering form is diverse [9]. Therefore, the inherent echo power fluctuation and maneuver characteristics of bird targets increase the difficulty of radar tracking processing.

For the problem of track breakages caused by the fluctuation of target echo power, an effective way is to set a reasonable detection threshold to balance false alarm and missed detection and achieve excellent tracking performance. In [10], an important relationship between detection thresholds and tracker performance has been established. More specifically, a modified Riccati equation (MRE) has been derived to describe the quantitative relationship between the tracker's error covariance and detection parameters to optimize the overall performance. However, the optimal operating point is only available via extensive numerical simulation. Further, an analytic approximation to MRE is presented in [11], which allows the precomputation of the estimation error covariance matrices and provides convenience for the solution of

* Corresponding author (email: lwd0539@163.com)

the optimal detection and tracking parameters. Based on this, a computationally efficient alternative solution for the special case of a Neyman-Pearson (NP) detector is proposed [12]. To suppress false alarm in the predicted gate, the Bayes detection is further introduced to probabilistic data association filter (PDAF) [13]. The threshold varies according to the ratio of prior probabilities, and is lowered in the vicinity of the predicted location. However, for the above algorithms, the detection performance expression is based on Swerling-I target fluctuation and is not suitable for the fluctuation characteristics of bird targets. In addition, they are only designed for single-target scenarios and do not consider maneuvers.

To deal with the maneuvering movement in multitarget tracking (MTT) scenarios, interacting multiple model (IMM) filter is generally combined with the Bayesian probabilistic data association algorithm, such as joint probabilistic data association and multiple hypothesis tracking (MHT) [14]. However, the Bayesian probabilistic data association algorithm costs a large computation [15], and the introduction of IMM increases the calculation burden. Besides, the multiple model approach has also been incorporated into random finite set based multitarget tracking methods such as probability hypothesis density [16], cardinalized probability hypothesis density [17], multi-Bernoulli [18], and labeled multi-Bernoulli [19] filters to track maneuvering targets. However, the movement of birds is flexible and the movement model conversion frequency is high [20]. It is difficult to obtain sufficient information to predefine multiple models [21]. Meanwhile, in terms of the single maneuvering model, the “current” statistical (CS) filtering model [22] has been proven to have excellent tracking performance. Here, a modified Rayleigh density is adopted to describe the “current” probability density of acceleration. However, several parameters, such as maximum acceleration, still need to be preset and remain constant. In practice, mismatched models or parameters will degrade tracking performance. Therefore, for maneuver uncertainty scenarios, it is vital to realize the real-time adjustment of filtering parameters in accordance with the motion state of each target.

Given that the existing MTT algorithms are difficult to simultaneously cope with the fluctuation and maneuver of bird target tracking, we proposed an MHT-based robust tracking method (RTM). The main contributions are summarized as follows.

- Based on the echo power fluctuation model of bird targets, the optimal detection operating point in the predicted gate is solved by a tracking feedback mechanism. Then, the measurement set reconstruction is realized to solve the track breakages caused by the echo power fluctuation.
- An adaptive parameter CS filter model is designed to improve the adaptability to maneuvering movement of bird targets.

The remainder of this paper is structured as follows. Section 2 presents the principle of the proposed RTM for bird targets. Simulation results and experiment data verification are analyzed in Sections 3 and 4, respectively. A summary of the work and conclusion are presented in Section 5.

2 The RTM based on target characteristics

The bird target tracking with fluctuation and maneuver characteristics involves the joint detection and estimation of a time-varying and unknown number of targets. Therefore, an effective MTT process framework is essential to achieve the stable tracking of bird targets. MHT [15] is capable of unifying the initiation and maintenance of the tracks in a framework and generally considered as the preferred method in the modern MTT system. However, there are two main challenges when bird target tracking copes with an MHT framework.

First, the information from detector to tracker flows only one way. Fluctuating echo power is likely to result in measurement loss for the existing tracks and mislead the tracking system to prematurely declare the track termination. Second, the movement is flexible and changeable. The widely used IMM-MHT algorithm is difficult to pre-define the model set and has large calculations.

Therefore, we developed RTM under the MHT-based MTT processing framework. The flow diagram is shown in Figure 1. For the sake of accommodating the bird target’s fluctuation and maneuver characteristics, four processing modules are designed and embedded into the MHT framework, as shown in the grey boxes.

2.1 Analysis of fluctuation characteristics of bird targets

The echo power of birds is affected by various factors and these factors are usually unknown and time varying [23]. Thus, it is always viewed as a random variable to describe the target fluctuating character-

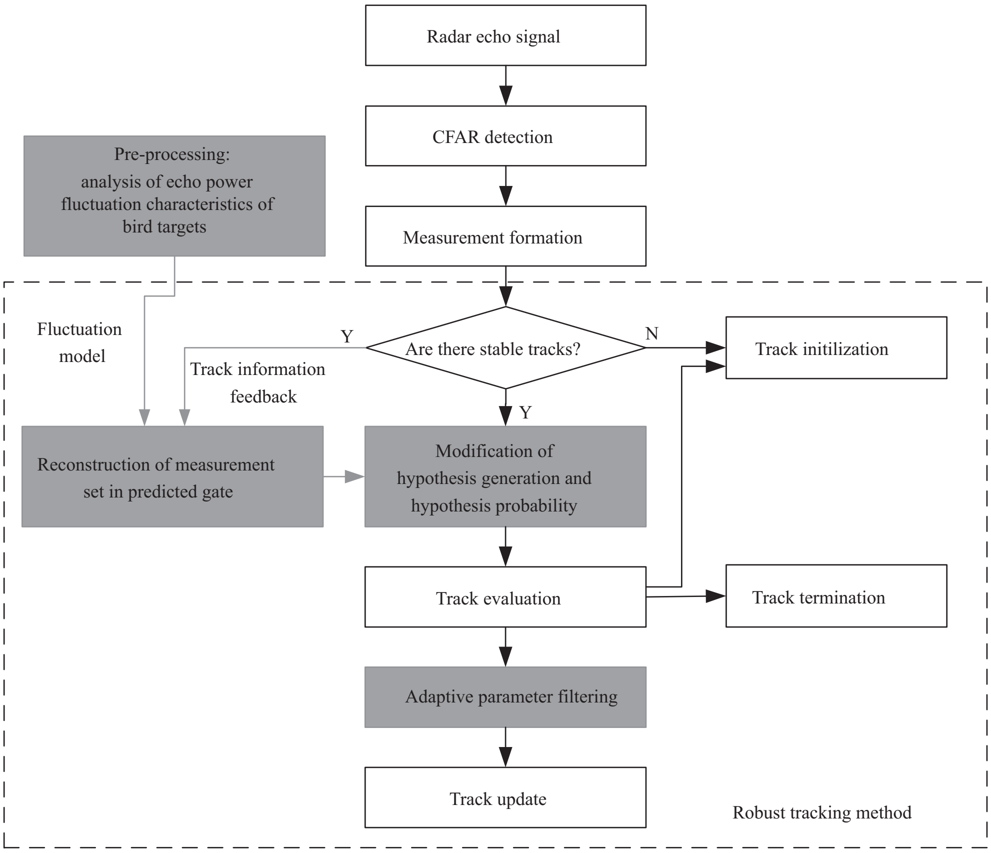

Figure 1 Flow diagram of the proposed RTM.

istics [24]. In this subsection, the fluctuating target echo power is modeled based on the data collected by the radar in a bird observation experiment. The experimental location and parameters are detailed in Section 4.

Specifically, 1364 groups of bird target tracks, including the echo power information, were extracted from experimental field data. The number of sampling points for each group is greater than 200. We employ five widely used distribution functions to model the echo power of bird targets: single parameter exponential distribution, dual parameter lognormal distribution, Weibull distribution, Gamma distribution, and normal distribution. The accuracy of model fitting is evaluated by K-S goodness-of-fit testing method [24].

Under the condition that the confidence level is taken as 0.05, the judgment result is shown in Figure 2. The values on the vertical axis represent the percentage of the track count that meets the corresponding distribution function to the total number of groups. Among the five distribution functions, Weibull distribution accounts for the highest proportion of 72%. Therefore, in this paper, we deem that the Weibull distribution model can well describe the echo power fluctuating characteristics of bird targets. Its probability distribution function (PDF) expression is given as follows:

$$p(x) = \left(\frac{\beta}{\eta}\right)\left(\frac{x}{\eta}\right)^{\beta-1} \mathrm{e}^{-\left(\frac{x}{\eta}\right)^{\beta}} \quad (x > 0), \tag{1}$$

where η is the scale parameter and β is the shape parameter.

2.2 Reconstruction of measurement set in predicted gate

In case the track breakages caused by echo power fluctuation, a measurement set reconstruction module is designed, and the processing flowchart is shown in Figure 3.

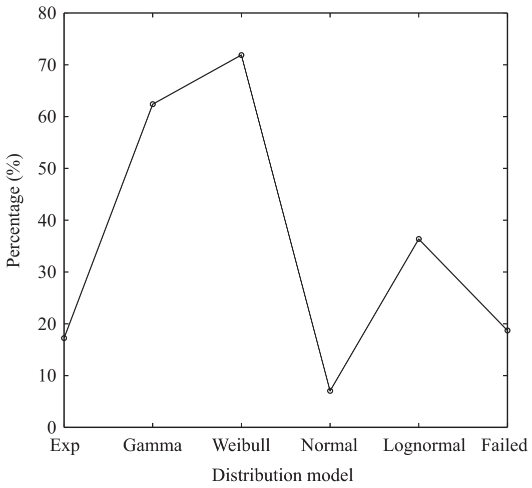

Figure 2 Judgment result of the K-S goodness-of-fit test.

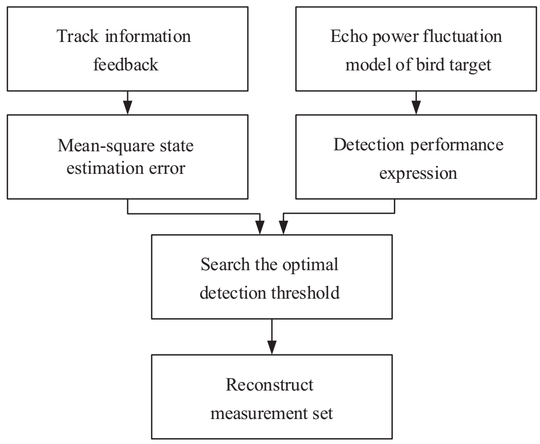

Figure 3 Flowchart of measurement set reconstruction.

2.2.1 *Detection performance expression based on Weibull fluctuation model*

In the detection process, we assume that a test of the absence or presence of a target at l-th resolution cell is performed. Hypothesis H_0 is that there is no target in the l-th resolution cell, and the measured return is simply noise. Hypothesis H_1 is that there is a target in the l-th resolution cell, and the return is a combination of noise and signal energy, which follows Weibull distribution with the scale parameter η and shape parameter β for bird targets. Under these two assumptions, the model of the observation signal can be written as follows:

$$p(a_l(k)|H_0) = \mathrm{e}^{-a_l(k)}, \tag{2}$$

$$p(a_l(k)|H_1) = \left(\frac{\beta}{\eta}\right)\left(\frac{a_l(k)}{\eta}\right)^{\beta-1} \mathrm{e}^{-\left(\frac{a_l(k)}{\eta}\right)^{\beta}}, \tag{3}$$

where $a_l(k)$ represents the echo power (magnitude-square output of a matched filter) of the l-th resolution cell at time k. If the threshold of the l-th resolution cell is τ, according to the Neyman-Pearson criterion, the test is expressed as follows:

$$a_l(k) \underset{H_0}{\overset{H_1}{\gtrless}} \tau. \tag{4}$$

The corresponding false alarm probability expression is

$$P_{\mathrm{FA}} = \int_{\tau}^{\infty} \mathrm{e}^{-a} \mathrm{d}a = \mathrm{e}^{-\tau}, \tag{5}$$

and the detection probability expression with the Weibull fluctuation model is

$$P_D = \int_{\tau}^{\infty} \left(\frac{\beta}{\eta}\right)\left(\frac{a}{\eta}\right)^{\beta-1} \mathrm{e}^{-\left(\frac{a}{\eta}\right)^{\beta}} \mathrm{d}a = \mathrm{e}^{-\left(\frac{\tau}{\eta}\right)^{\beta}}. \tag{6}$$

2.2.2 *Optimal detection threshold calculation and measurement set reconstruction*

A feedback mechanism from the tracking subsystem to the detection subsystem is provided to ensure stable tracking when the target echo power fluctuates. The MRE is used in conjunction with the detection performance expression to determine the detection threshold and achieve optimal tracking performance [25]. Specifically, the conditional mean-square state estimation error at time k is minimized over detection thresholds at time k given Z^{k-1} (data up to time $k-1$). Suppose P_D and P_{FA} are parameterized by a detection threshold τ, i.e., $P_D = P_D(\tau, \eta, \beta)$, $P_{\mathrm{FA}} = P_{\mathrm{FA}}(\tau)$ for $\tau \in \Theta$. Then, we aim to solve the problem

$$\begin{aligned} &\tau^*(k) = \arg\min_{\tau} \left\{ E\left[\|X(k) - \hat{X}(k \mid k)\|^2 \mid Z^{k-1} \right] \right\} \\ &\text{s.t. } \tau \in \Theta, \end{aligned} \tag{7}$$

where $X(k)$ is the state vector including position and velocity variables, and $\hat{X}(k \mid k)$ is the state estimate.

Based on [12], we have

$$E\left[\|X(k)-\hat{X}(k \mid k)\|^2 \mid Z^{k-1}\right]=\operatorname{tr}\left\{E\left[P(k \mid k) \mid Z^{k-1}\right]\right\}, \tag{8}$$

where $P(k \mid k)$ is a covariance coming from an update equation. Thus, it is vital to obtain a measurement-independent recursion for the covariance of the filter. MRE is derived in [10], as a deterministic approximation to the stochastic error covariance update equation. For time-invariant systems, MRE can be iterated forward in time, and an estimate of the steady-state error covariance can be produced. Thus, we obtain

$$E\left[P(k \mid k) \mid Z^{k-1}\right]=P(k \mid k-1)-q_2\left(P_{\mathrm{FA}} N_c(k), P_D\right) W(k) S(k) W^{\mathrm{T}}(k), \tag{9}$$

where $W(k)$ and $S(k)$ are the filtering gain and innovation covariance, respectively. The time-varying scalar $q_2\left(P_{\mathrm{FA}} N_c(k), P_D\right)$ is called information reduction factor (IRF) [10], which lies between 0 and 1. $N_c(k) \triangleq V(k)/V_c$ is the number of resolution cells enclosed by the validation gate at time k, where $V(k)$ is the offline-calculated gate volume and V_c is the resolution unit volume.

Substituting (9) into (8), we obtain

$$E\left[\|X(k)-\hat{X}(k \mid k)\|^2 \mid Z^{k-1}\right]=\operatorname{tr}\{P(k \mid k-1)\}-q_2\left(P_{\mathrm{FA}} N_C(k), P_D\right) \operatorname{tr}\left\{W(k) S(k) W^{\mathrm{T}}(k)\right\}. \tag{10}$$

Since $W(k)S(k)W^{\mathrm{T}}(k) \geqslant 0$ implies $\operatorname{tr}\{W(k)S(k)W^{\mathrm{T}}(k)\} \geqslant 0$, if $q_2(\cdot)$ is maximized, $E[\|X(k)-\hat{X}(k \mid k)\|^2 \mid Z^{k-1}]$ will be minimized. Therefore, the optimization problem in (7) becomes:

$$\begin{aligned} & \tau^*(k)=\arg \max_\tau q_2\left(P_{\mathrm{FA}} N_C(k), P_D\right) \\ & \text{s.t. } \tau \in \Theta. \end{aligned} \tag{11}$$

However, the IRF given in (9) has no closed-form, and its analytic approximation is presented in [11] for the case of a two-dimensional measurement vector and a four sigma validation gate, as follows:

$$q_2\left(P_{\mathrm{FA}} N_C(k), P_D\right)=\frac{0.997 P_D}{1+0.37 N_C(k) P_D^{-1.57} P_{\mathrm{FA}}}. \tag{12}$$

Then, the optimal detection threshold can be solved according to the following steps.

Step 1. Taking the logarithm of both sides of (12), we obtain

$$\ln \left(q_2\left(P_{\mathrm{FA}} N_C(k), P_D\right)\right)=\ln \left(0.997 P_D\right)-\ln \left(1+0.37 \mathrm{~N}_C(k) P_D^{-1.57} P_{\mathrm{FA}}\right). \tag{13}$$

Here, when the track is in the stable tracking stage, we can make the following assumptions. False alarm probability is generally not greater than 10^{-2}, and the detection probability is greater than 0.5 and less than 1. Additionally, $N_C(k)$ is the number of resolution cells enclosed by the validation gate and less than 50. Thus, on the right hand side of (13), the second term $\ln(1+0.37 \mathrm{~N}_C(k) P_D^{-1.57} P_{\mathrm{FA}})$ can be approximated as $0.37 \mathrm{~N}_C(k) P_D^{-1.57} P_{\mathrm{FA}}$. Then, we obtain

$$\ln \left(q_2\left(P_{\mathrm{FA}} N_C(k), P_D\right)\right) \approx \ln \left(0.997 P_D\right)-0.37 \mathrm{~N}_C(k) P_D^{-1.57} P_{\mathrm{FA}}. \tag{14}$$

Step 2. Incorporating the false alarm probability and detection probability defined in (5) and (6) into (14), we obtain

$$\ln \left(q_2\left(\tau, N_C(k), \eta, \beta\right)\right)=\ln (0.997)-\left(\frac{\tau}{\eta}\right)^\beta-0.37 N_C(k) \exp \left(1.57\left(\frac{\tau}{\eta}\right)^\beta-\tau\right). \tag{15}$$

Step 3. Since taking the logarithm does not affect the monotonicity of the function, the optimization problem in (11) can be transformed as follows:

$$\begin{aligned} & \tau^*(k)=\arg \max_\tau \ln \left(q_2\left(\tau, N_C(k), \eta, \beta\right)\right) \\ & \text{s.t. } \tau \in \Theta. \end{aligned} \tag{16}$$

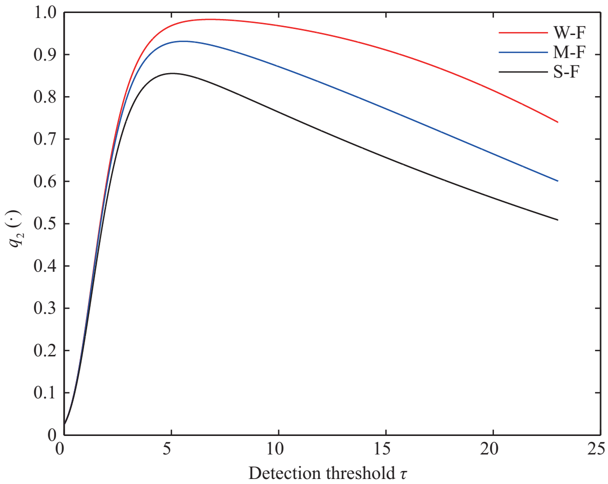

Figure 4 (Color online) Variation of $q_2(\tau, N_C, \eta, \beta)$ for $Nc = 10$, and SNR = 15 dB with different fluctuation levels. W-F, M-F, and S-F indicate weak, medium, and strong fluctuations, respectively.

Step 4. Based on the simulation in Figure 4, we can verify that, given the fluctuation model parameters η, β, and $N_C(k)$, $\ln(q_2(\cdot))$ is unimodal with respect to τ and has a single local maximum. Therefore, the optimal detection threshold is found by taking the derivative of (15) with respect to τ and equating the result to 0. After some rearrangements, the optimal detection threshold τ^* can be solved by dichotomy based on the following equation:

$$f(\tau) = -\left(\frac{\beta}{\eta}\right)\left(\frac{\tau}{\eta}\right)^{\beta-1} - 0.37N_C(k)\left(1.57\left(\frac{\beta}{\eta}\right)\left(\frac{\tau}{\eta}\right)^{\beta-1} - 1\right)\exp\left(1.57\left(\frac{\tau}{\eta}\right)^{\beta} - \tau\right) = 0. \tag{17}$$

Then, the target track information, including the predicted gate location and size, is fed back to the detection module, and the corresponding range resolution cells are detected by threshold $\tau^*(k)$. The measurements obtained in the predicted gate of all tracks at time k are denoted as the reconstructed measurement set.

2.3 Modification of hypothesis generation and hypothesis probability calculation

The measurement set reconstruction improves the detection probability for fluctuating echo power, whereas it may bring a high false alarm probability. Therefore, to avoid the increase in false measurements resulting in a high calculation burden and poor data association accuracy, the hypothesis generation and hypothesis probability calculation modules of the MHT processing are modified based on measurement origin constraints.

2.3.1 *Hypothesis generation*

Let $Z(k) = \{z_i(k)\}_{i=1}^{m_k}$ denote the measurement set at time k, where, m_k is the total number of measurements; $Z^k \triangleq \{Z(1), Z(2), \ldots, Z(k)\}$ denote the cumulative measurement set up to time k; $\Omega^k \triangleq \{\Omega_i^k, i = 1, 2, \ldots, J_k\}$ denote the set of all hypotheses at the time k, which associate the cumulative set of measurements Z^k with targets or clutter [15].

According to the measurement origins, the number of measurements from the CFAR detection module is denoted as m_k^f. For the reconstructed measurement set, suppose the existing stable track index set at the time k is $T(k) = \{t_r\}, r \in \{1, 2, \ldots, N\}$, and N is the total number of tracks. The number of reconstructed measurements in the predicted gate of track t_r is denoted as m_k^r. Thus, the total number of measurements at time k is given by

$$m_k = m_k^f + \sum_{r=1}^{N} m_k^r. \tag{18}$$

Based on the above analysis, the hypothesis sets Ω^k are updated for Ω^{k-1} and each measurement $z_i(k)$. For $z_{fi}(k)$, $fi = 1, 2, \ldots, m_k^f$, the possible origin is as follows: (i) track continuation; (ii) new target;

Table 1 Notations for measurements from CFAR detection module

Notation	Meaning
τ_f^i	The indicator function for the assignment of measurement $z_{fi}(k)$ to a track
v_f	The number of measurements deemed as new targets
δ_t	The indicator function for the assignment of a measurement to track t
ϕ_f	The number of measurements deemed as false alarms $\phi_f = m_k^f - \tau_f - v_f$
V	The surveillance volume
f_{ti}	The PDF of the predicted location of track t to which measurement $z_{fi}(k)$ is assigned in the hypothesis under consideration
P_D^t	The detection probability of target t

(iii) false alarm. For $z_{ri}(k),\ ri = 1, 2, \ldots, m_k^r$, the possible origin is as follows: (i) track t_r continuation; (ii) false alarm.

2.3.2 *Hypothesis probability calculation*

MHT technique [15] evaluates the probabilities of sequences of measurements originating from different targets by setting up all possible hypotheses as continuations of the hypotheses at the previous sampling time. The hypothesis probability is also corrected based on the measurement origin constraints.

• For $z_{fi}(k),\ fi = 1, 2, \ldots, m_k^f$, the notations used [26] are listed in Table 1. The joint event probability corresponding to this part of measurements can be expressed as follows:

$$P_f = \frac{1}{C_f}\frac{v_f!\phi_f!}{m_k^f!}\mu_{\phi_f}\left(\phi_f\right)\mu_{v_f}\left(v_f\right)V^{-\phi_f - v_f}\prod_{i=1}^{m_k^f}\left\{f_{ti}\left[z_{fi}(k)\right]\right\}^{\tau_f^i}\prod_t\left(P_D^t\right)^{\delta_t}\left(1-P_D^t\right)^{1-\delta_t}, \tag{19}$$

where C_f is the normalization constant. Generally, the number of false measurements assumes a Poisson probability mass function (pmf) with spatial density λ_{ϕ_f}, namely,

$$\mu_{\phi_f}\left(\phi_f\right) = \mathrm{e}^{-\lambda_{\phi_f}V}\frac{\left(\lambda_{\phi_f}V\right)^{\phi_f}}{\phi_f!}. \tag{20}$$

Similarly, for the number of new targets, with spatial density λ_{v_f}, we have

$$\mu_{v_f}\left(v_f\right) = \mathrm{e}^{-\lambda_{v_f}V}\frac{\left(\lambda_{v_f}V\right)^{v_f}}{v_f!}. \tag{21}$$

Note that λ_{ϕ_f} and λ_{v_f} are measurement spatial density, i.e., the expected number of false and new target measurements per unit volume of the measurement space per frame respectively. It can be calculated by [26]

$$\lambda_\phi = P_{\mathrm{FA}}/V_C. \tag{22}$$

Therefore, when the false alarm probability is constant as P_{FA}, the false measurement spatial density is also constant as λ_{ϕ_f}.

• For $z_{ri}(k),\ ri = 1, 2, \ldots, m_k^r$, the difference is that the track t_r definitely exists and this part of measurements lie in the predicted gate of track t_r. The notations used are presented in Table 2. The joint event probability corresponding to this part of measurements can be expressed as follows:

$$P_r = \frac{1}{C_r}\frac{\phi_r!}{m_k^r!}\mu_{\phi_r}\left(\phi_r\right)V^{-\phi_r}\prod_{i=1}^{m_k^r}\left\{f_{t_r i}\left[z_{ri}(k)\right]\right\}^{\tau_r^i}P_D^{t_r}, \tag{23}$$

where C_r is the normalization constant.

As discussed in Subsection 2.2.2, we know that the optimal detection threshold in the predicted gate is time-varying. The corresponding false alarm probability can be calculated using (5), and it is recorded as $P_{\mathrm{FA}}^r(k)$. Then, the modified false measurement spatial density calculated using (22) is denoted as $\lambda_{\phi_r}(k)$. Therefore, the pmf of the number of false alarms in the current frame is represented as

$$\mu_{\phi_r}\left(\phi_r\right) = \mathrm{e}^{-\lambda_{\phi_r}(k)V}\frac{\left(\lambda_{\phi_r}(k)V\right)^{\phi_r}}{\phi_r!}. \tag{24}$$

Table 2 Notations for measurements from reconstruction module

Notation	Meaning
τ_r^i	The indicator function for the assignment of measurement $z_{ri}(k)$ to a track t_r
δ_{t_r}	The indicator function for the assignment of a measurement to track t_r and certainly equal to 1
ϕ_r	The number of measurements deemed as false alarms $\phi_r = m_k^r - \tau_r$

As discussed above, the probability of the joint association hypothesis l through the current time k is modified as follows:

$$\Pr\left\{\Omega^{k,l} \mid Z^k\right\} = P_f \cdot \prod_{r=1}^{N} P_r. \tag{25}$$

2.4 Adaptive parameter "current" statistical filtering model

The CS filtering model [22] is adaptive and can estimate well the states of highly maneuvering targets. However, for the traditional CS model, some filtering parameters, such as maneuvering frequency and maximum acceleration, should be predetermined with experience and generally assumed to remain constant in the filtering process. The unreasonable initial parameter configuration can lead to poor tracking performance. Therefore, an adaptive parameter adjustment strategy is proposed to better accommodate the uncertain maneuvering movement of bird targets.

2.4.1 *The "current" statistical model*

The CS model of discrete state equation [22] is given as follows:

$$X(k+1) = F(k)X(k) + G(k)\bar{a}(k) + v(k), \tag{26}$$

where kinematics state $X(k) = [\, x(k) \;\; \dot{x}(k) \;\; \ddot{x}(k)\,]^{\mathrm{T}}$,

$$F(k) = \begin{bmatrix} 1 & T & (-1+\alpha T + \mathrm{e}^{-\alpha T})/\alpha^2 \\ 0 & 1 & (1-\mathrm{e}^{-\alpha T})/\alpha \\ 0 & 0 & \mathrm{e}^{-\alpha T} \end{bmatrix}, \tag{27}$$

$$G(k) = \begin{bmatrix} (-T+\alpha T^2/2 + (1-\mathrm{e}^{-\alpha T})/\alpha)/\alpha \\ T-(1-\mathrm{e}^{-\alpha T})/\alpha \\ 1-\mathrm{e}^{-\alpha T} \end{bmatrix}. \tag{28}$$

Here, T is the sampling period, and $v(k)$ is a discrete time white noise sequence with variance $2\alpha\sigma_a^2$; α is the maneuvering frequency; σ_a^2 is the acceleration variance calculated using the following equation:

$$\sigma_a^2 = \frac{4-\pi}{\pi}[a_{\max} - \bar{a}(k)]^2, \tag{29}$$

$$\bar{a}(k) = \hat{\ddot{x}}(k|k-1), \tag{30}$$

where $\bar{a}(k)$ is the acceleration mean value, and $a_{\max}$ is the acceleration limit of the target.

The observation equation can be written as follows:

$$Z(k) = H(k)X(k) + w(k), \tag{31}$$

where $H(k) = [1 \;\; 0 \;\; 0]$, and $w(k)$ is Gaussian with zero-mean and variance $R(k)$.

2.4.2 *Acceleration variance adaptive adjustment strategy*

From (29), we obtain that the maximum acceleration $a_{\max}$ directly affects the acceleration variance σ_a^2. However, in practice it is hard to pre-define. Therefore, we estimate σ_a^2 online based on the relationship between the innovation and acceleration variation [27].

Specifically, if the filtering model is completely matched with the movement model, and according to the displacement formula, the one-step predicted state satisfies

$$x(k|k-1) = \hat{x}(k-1) + \hat{\dot{x}}(k-1)T + 1/2\hat{\ddot{x}}(k-1)T^2. \tag{32}$$

In practice, the observation state is given by

$$z(k) = \hat{x}(k-1) + \hat{\dot{x}}(k-1)T + 1/2\big(\hat{\ddot{x}}(k-1) + \tilde{a}(k)\big)T^2 + w(k). \tag{33}$$

Here, $w(k)$ is the random error of sensor observation at time k, which is Gaussian white noise with zero-mean, i.e., $E\{w(k)\} = 0$; $\tilde{a}(k)$ is the acceleration variation due to target maneuvering. The innovation, i.e., the difference between the prediction and observation state, can be expressed as follows:

$$\Delta d(k) = \frac{1}{2}\tilde{a}(k)T^2 + w(k). \tag{34}$$

Therefore, the innovation $\Delta d(k)$ includes the acceleration variation and the random error of the sensor observation. Since they are independent, we obtain

$$E\{\Delta d(k)\} = E\left\{\frac{1}{2}\tilde{a}(k)T^2\right\} + E\{w(k)\}. \tag{35}$$

When the target is moving at a constant acceleration, the estimated acceleration is basically the same as the actual value, and the change in acceleration is Gaussian with zero mean, $E\{\tilde{a}\} = 0$. At this point, $E\{\Delta d\} = 0$. However, target movement is usually maneuverable and the acceleration is time-varying, i.e., $E\{\tilde{a}\} \neq 0$, and

$$E\{\Delta d(k)\} = E\left\{\frac{1}{2}\tilde{a}(k)T^2\right\}. \tag{36}$$

Suppose the acceleration variance σ_a^2 is linearly related to $\tilde{a}(k)$, i.e., $\sigma_a^2(k) \to |\tilde{a}(k)|$. Based on (36), we obtain

$$\sigma_a^2(k) = \frac{2}{T^2}E\{\Delta d(k)\}. \tag{37}$$

This means that when the maneuver occurs, the acceleration variance increases as the innovation becomes larger, which is consistent with the target movement.

2.4.3 *Maneuvering frequency adaptive adjustment strategy*

The physical meaning of maneuvering frequency α can be understood as the reciprocal of the target maneuvering time constant. We modify the maneuvering frequency at the current time with a weighting factor derived from the relative acceleration variation of the historical times. Meanwhile, to ensure the accurate response of the maneuver, a time reference window is set. The length can be defined according to the sampling periods and practical observation scenarios.

Specifically, the acceleration variation at time k is defined as follows:

$$\Delta a(k) = \mathrm{abs}\left(\hat{a}(k) - \hat{a}(k-1)\right), \tag{38}$$

where $\hat{a}(k) = \ddot{x}(k)$ is the estimated acceleration at time k. Define the length of the reference window is T_c. Thus, the number of frames in the reference window is $F_{\mathrm{Num}} = \mathrm{round}(T_c/T)$. The sets of acceleration variation, from the start of the reference window to frame $k-1$, is defined as $A^{k-1} = \{\Delta a(k-F_{\mathrm{Num}}), \Delta a(k-F_{\mathrm{Num}}+1), \ldots, \Delta a(k-1)\}$. The maximum value in A^{k-1} is chosen and represented as $\Delta a_{\max}$.

The maneuvering frequency weighting factor at time k is defined by

$$WF_\alpha(k) = \frac{\Delta a(k)}{\Delta a_{\max}}. \tag{39}$$

Then the maneuvering frequency at time k can be modified as follows:

$$\alpha(k) = WF_\alpha(k) \times \alpha(k-1). \tag{40}$$

3 Simulation results

3.1 Performance measures

In this subsection, we present several performance measures used to evaluate the proposed RTM.

(1) Success tracking ratio (STR). If a track can maintain more than N_T frames and ensure that the mean of the tracking error is less than the standard deviation of measurement noise σ_w, the trajectory is considered to be tracked successfully, i.e., satisfying

$$\frac{1}{N_T}\sum_{k=1}^{N_T}|\hat{x}(k)-x(k)| \leqslant \sigma_w, \tag{41}$$

where $\hat{x}(k)$ is the state estimation at time k, and $x(k)$ is the real value.

(2) Cumulative number of track breakages (CNTB). The total number of frames that the true target is not assigned to the track before the evaluation time $t_{\rm eval}$ is called the cumulative number of track breakages at time $t_{\rm eval}$, denoted as $\mathrm{CNTB}(t_{\rm eval})$ [28] and defined by

$$\mathrm{CNTB}(t_{\rm eval}) = \frac{1}{L}\sum_{r=1}^{L}\mathrm{CNTB}_r(t_{\rm eval}), \tag{42}$$

where L is the total number of true targets, and $\mathrm{CNTB}(t_{\rm eval})$ is the total number of track breakages of the true target r until the evaluation time $t_{\rm eval}$.

(3) The MOSPA metric. The optimal subpattern assignment (OSPA) metric evaluates the overall tracking performance of an MTT algorithm. The calculation details are contained in [29]. In the following simulation, the configuration values $p = 1$ and $c = 100$ m are used. To compare the tracking accuracy more intuitively, we take the average of OSPA in the stable tracking stage. The MOSPA is defined as

$$\mathrm{MOSPA} = \frac{1}{T_E - T_S + 1}\sum_{k=T_S}^{T_E}\mathrm{OSPA}(k), \tag{43}$$

where T_S and T_E are the start and end frames of the stable track stage, respectively.

(4) Running time. To assess the computational requirements of the proposed method, the running time is obtained by computing the averaged CPU time in MATLAB 2017 on an Intel Core 2.40 GHz 2CPU computer operating under Windows 10.

3.2 Simulation parameters design

To simulate the movement trajectory of bird targets and facilitate the performance evaluation of the algorithm, we use the maneuvering index defined in [30] to describe the maneuvering level of the target movement.

The maneuvering index is given by

$$\lambda = \frac{\sigma_v T^2}{\sigma_w}, \tag{44}$$

where σ_v is the process noise standard deviation, and σ_w is the measurement noise standard deviation.

The simulation parameters are designed as follows:

• The sampling period T of the sensor is fixed at 1 s.

• The measurement noise standard deviation σ_w is fixed at 7 m.

• The maneuvering level is adjusted by changing the process noise standard deviation σ_v.

• The echo power fluctuation of the range cell, where a target is located, follows the Weibull distribution model. The model parameter η and β determine the echo power fluctuating level and are calculated using the maximum likelihood estimation.

• The number of Monte Carlo simulation runs is 500.

Since the analytic approximation of IRF $q_2(\tau, N_C, \eta, \beta)$ in (17) is related to multiple uncertain parameters of N_C, η, and β, we verify its monotonicity under several sets of practical values. Given the signal-to-noise ratio (SNR) mean value is 15 dB, model parameter η and β are set according to the fluctuating levels defined in Table 3, and $N_C = 10$. The detection threshold τ corresponds to the $P_{\rm FA}$ domain of interest $[10^{-10}, 1]$. The simulation result is shown in Figure 4. It can be clearly seen that $q_2(\cdot)$ has a single local maximum.

Table 3 Fluctuating and maneuvering parameters design

	Fluctuating level		
	Weak	Medium	Strong
SNR standard deviation/dB	2	3.5	5
	Maneuvering level		
	Weak	Medium	Strong
Maneuvering index	0.2	1	2

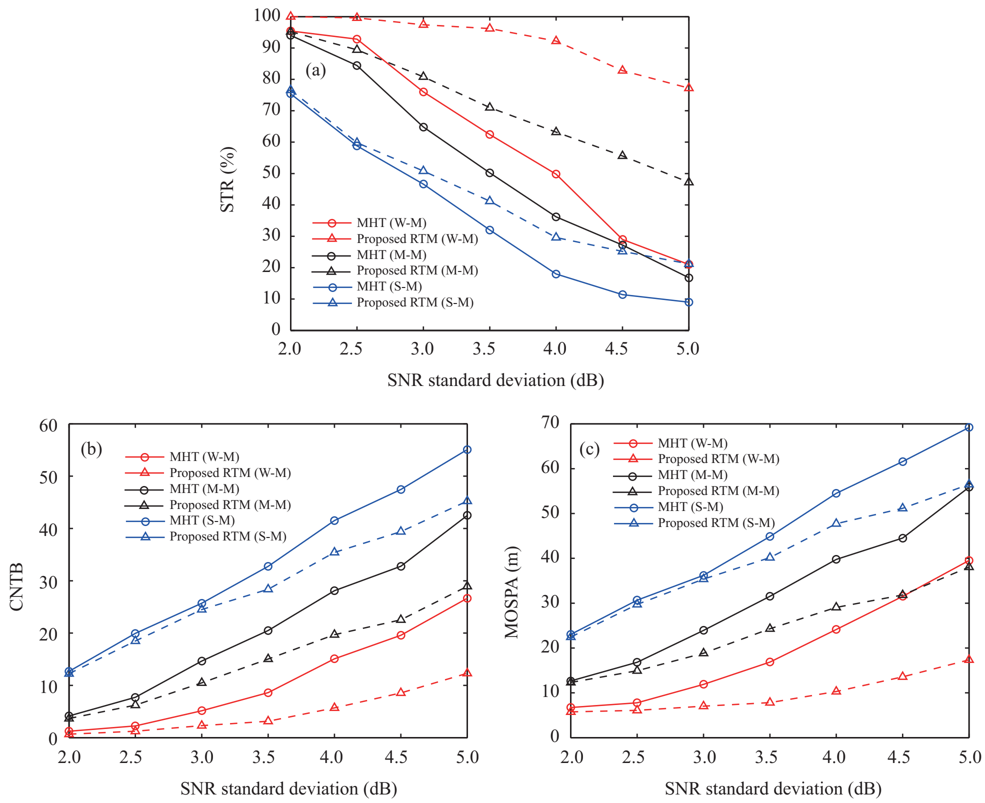

Figure 5 (Color online) Performance comparison of different fluctuating levels. (a) STR; (b) CNTB; (c) MOSPA. W-M, M-M, and S-M indicate weak, medium, and strong maneuver, respectively.

3.3 Result comparisons

Simulation scenarios with different fluctuating levels, maneuvering levels, SNR mean values and the number of targets are constructed to evaluate the tracking performance of the proposed RTM. The influences of fluctuation, maneuver and SNR are analyzed in a single target scenario. Then, several parameters are selected to verify the applicability in scenarios with different target numbers. For a fair comparison, the same CFAR detection process is adopted to ensure that MHT and RTM obtain the same measurements from the detection module, thereby verifying the robustness of the proposed RTM to the fluctuation. Additionally, the traditional CS model is adopted in the filter module of the MHT algorithm to verify the robustness of the proposed RTM to the maneuver.

3.3.1 *Performance at different fluctuating levels*

The initial target state is set as $[900\ \mathrm{m}, 15\ \mathrm{m/s}, 900\ \mathrm{m}, 15\ \mathrm{m/s}]^{\mathrm{T}}$. Given that the SNR mean value is 15 dB, by adjusting the parameters of the Weibull fluctuating model, the SNR standard deviation varies from 2 to 5 dB, with increments of 0.5 dB. Meanwhile, weak, medium and strong maneuvering levels corresponding to the maneuvering index defined in Table 3 are set.

Figure 5 shows that the tracking performance gradually decreases as the SNR standard deviation increases. As a concrete manifestation of an increase in the CNTB and MOSPA distance and decrease in STR. When the SNR standard deviation is less than 2.5 dB, regardless of the maneuvering level, the

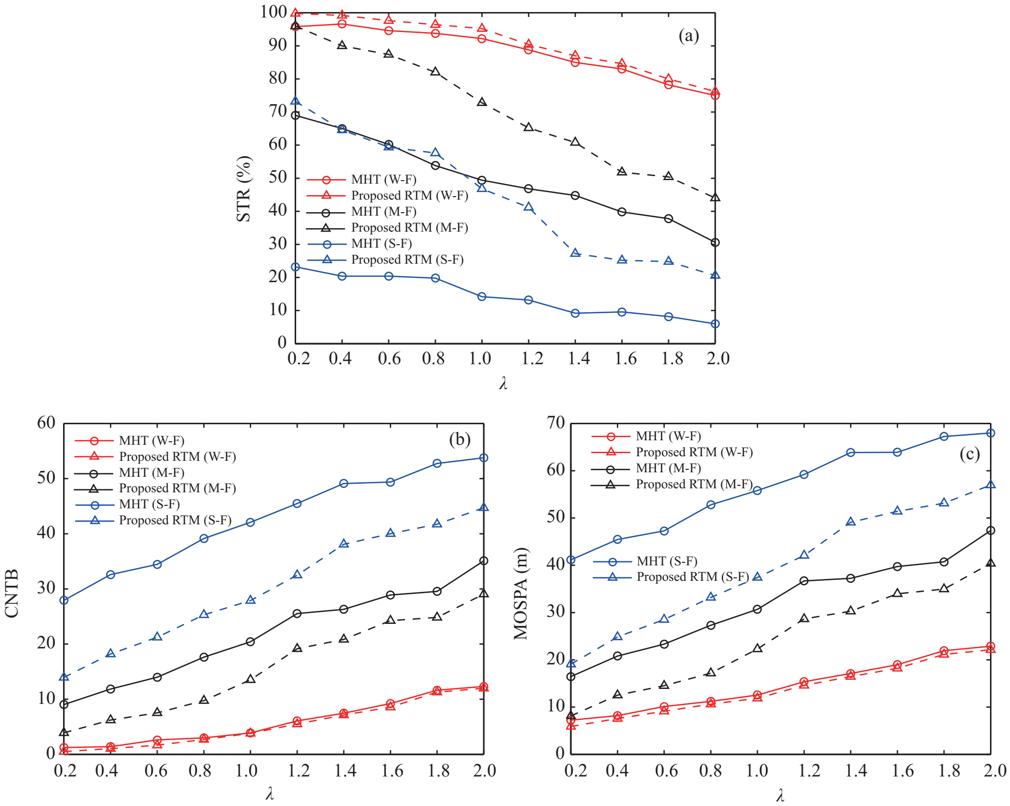

Figure 6 (Color online) Performance comparison of different maneuvering levels. (a) STR; (b) CNTB; (c) MOSPA.

performance improvement of the proposed method is small. However, when the SNR standard deviation is greater than 2.5 dB, the performance improvement of the proposed method increases, which is the most significant in the case of weak maneuvers. For example, Figure 5(a) shows that when the SNR standard deviation is 5 dB, under weak maneuvering level, the STR of MHT is only 21%, whereas the proposed RTM can reach 77%, an increase of 56%. Additionally, from the perspective of vertical comparison, the proposed method is superior to the MHT algorithm. However, the tracking performance of the two algorithms decreases as the maneuvering level increases.

3.3.2 *Performance at different maneuvering levels*

The initial target state is set as $[900\ \mathrm{m}, 15\ \mathrm{m/s}, 900\ \mathrm{m}, 15\ \mathrm{m/s}]^{\mathrm{T}}$; the SNR mean value is 15 dB. The maneuvering index λ is changed by adjusting the process noise standard deviation σ_v according to (44), ranging from 0.2 to 2, with increments of 0.2. It means that, the process noise standard deviation σ_v ranges from 1.4 to 14 m/s^2 for the designed σ_w and T. Meanwhile, weak, medium and strong fluctuating levels corresponding to the parameters defined in Table 3 are set.

Figure 6 shows that the tracking performance deteriorates as the maneuvering level of the horizontal axis increases. In the case of weak fluctuation (as shown by the red line), the maneuvering level slightly affects the tracking performance. In the case of medium fluctuation (as shown by the black line), when $\lambda < 1$, the STR of the proposed method can be improved by about 27% at the maximum compared with MHT. However, when $\lambda > 1$, the performance improvement gradually reduces. In the case of strong fluctuation (as shown by the blue line), when $\lambda < 1$, the performance of the proposed method significantly improves compared with MHT. However, at this point, the performance is not ideal if the maneuver is too strong, although it has some improvement compared with MHT. This is because the detection probability decreases in the case of strong fluctuation, making it difficult to achieve optimal tracking performance.

3.3.3 *Performance at different SNR levels*

The initial target state is set as $[900\ \mathrm{m}, 15\ \mathrm{m/s}, 900\ \mathrm{m}, 15\ \mathrm{m/s}]^{\mathrm{T}}$, and the SNR varies from 12 to 18 dB, with increments of 1 dB. In addition to changing the maneuvering level, the fluctuating level is adjusted

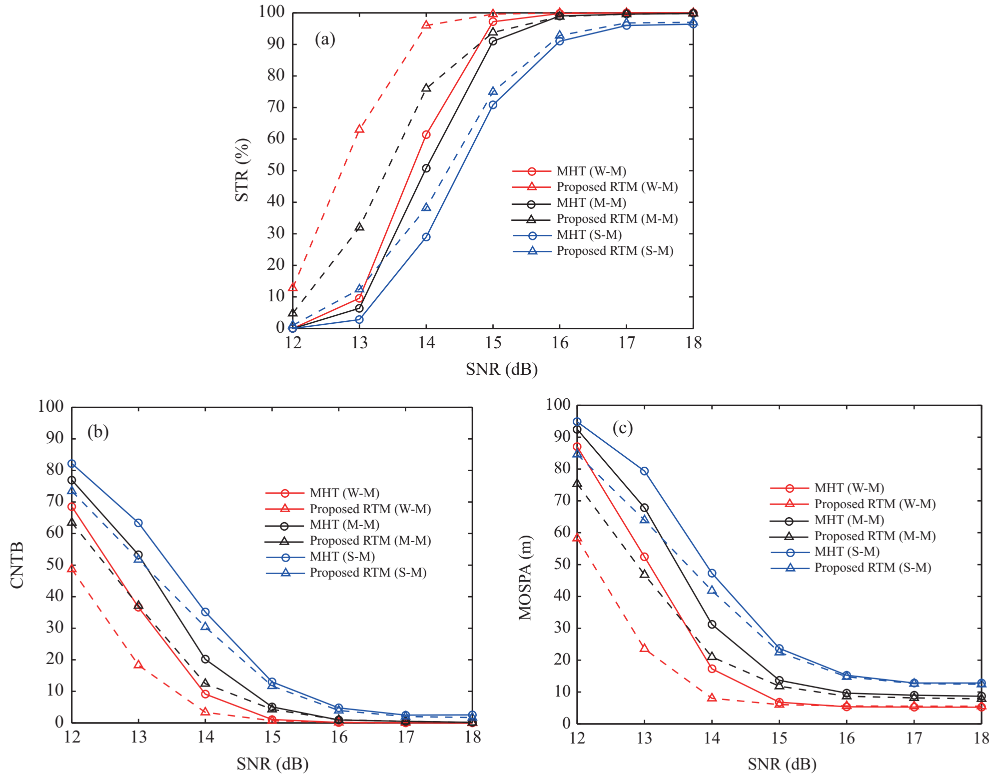

Figure 7 (Color online) Performance comparison of different SNR with weak fluctuation. (a) STR; (b) CNTB; (c) MOSPA.

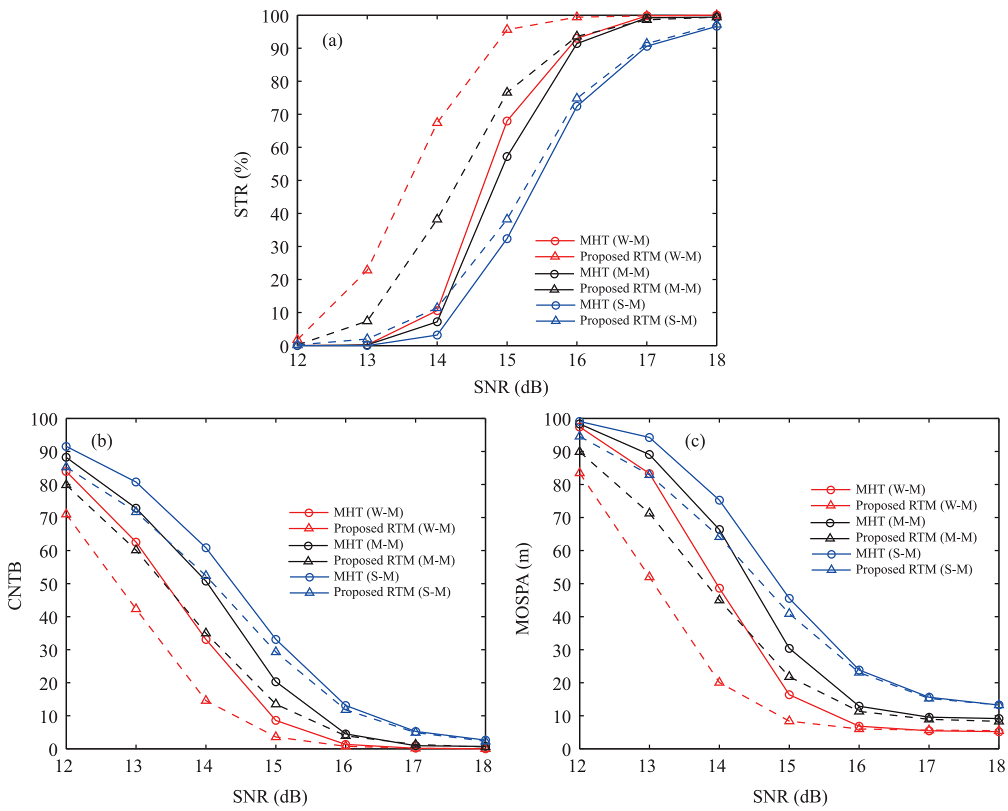

Figure 8 (Color online) Performance comparison of different SNR with medium fluctuation. (a) STR; (b) CNTB; (c) MOSPA.

simultaneously in each SNR level. Figures 7–9 show the performance comparison corresponding to weak,

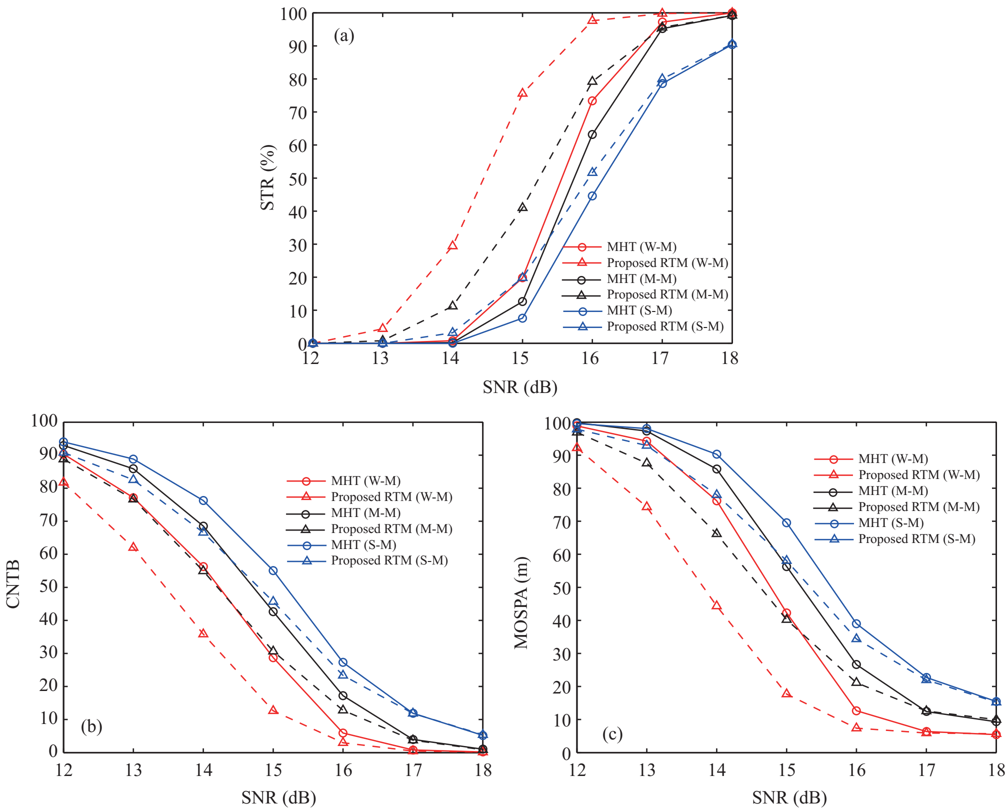

Figure 9 (Color online) Performance comparison of different SNR with strong fluctuation. (a) STR; (b) CNTB; (c) MOSPA.

Table 4 Parameter settings for typical scenarios

Scenario index	Fluctuating level	Maneuvering level
1	Weak	Weak
2	Weak	Strong
3	Strong	Weak
4	Strong	Strong

medium, and strong fluctuations, respectively.

First, regardless of the fluctuating and maneuvering level are strong or weak, the tracking performances gradually improve as SNR increases. However, the performance improvement of the proposed RTM increases first and then decreases compared with MHT. Second, the SNR required to achieve the same STR increases as the fluctuating level increases at the same maneuvering level. Meanwhile, the proposed RTM requires lower SNR than MHT. For example, for the proposed RTM, in the case of weak maneuver, when the fluctuating level is weak, medium and strong (shown by the red curve in the Figures 7(a), 8(a), and 9(a), respectively), the minimum SNR required to achieve an STR of over 90% is 14, 15, and 16 dB respectively. In contrast, the minimum SNR required to achieve the same for the MHT algorithm is 15, 16, and 17 dB, respectively. Figures 7–9 also show that increases in fluctuation and maneuver will result in varying degrees of degradation of tracking performance, and the fluctuating level has a greater impact, especially at low SNR levels.

3.3.4 *Performance at different target numbers*

Four typical scenarios shown in Table 4 are constructed to verify the tracking performance of the proposed method with different number of targets, and the performance comparisons are shown in Figure 10. The SNR mean value is 15 dB. The initial target states under different target numbers are selected sequentially from Table 5, where the velocity direction of the Y axis is changed to ensure that the trajectories cross. In each Monte Carlo simulation, the process noise is a Gaussian random variable with a given maneuvering level, and the target trajectories have randomness. Figure 11 shows a schematic of a set of randomly

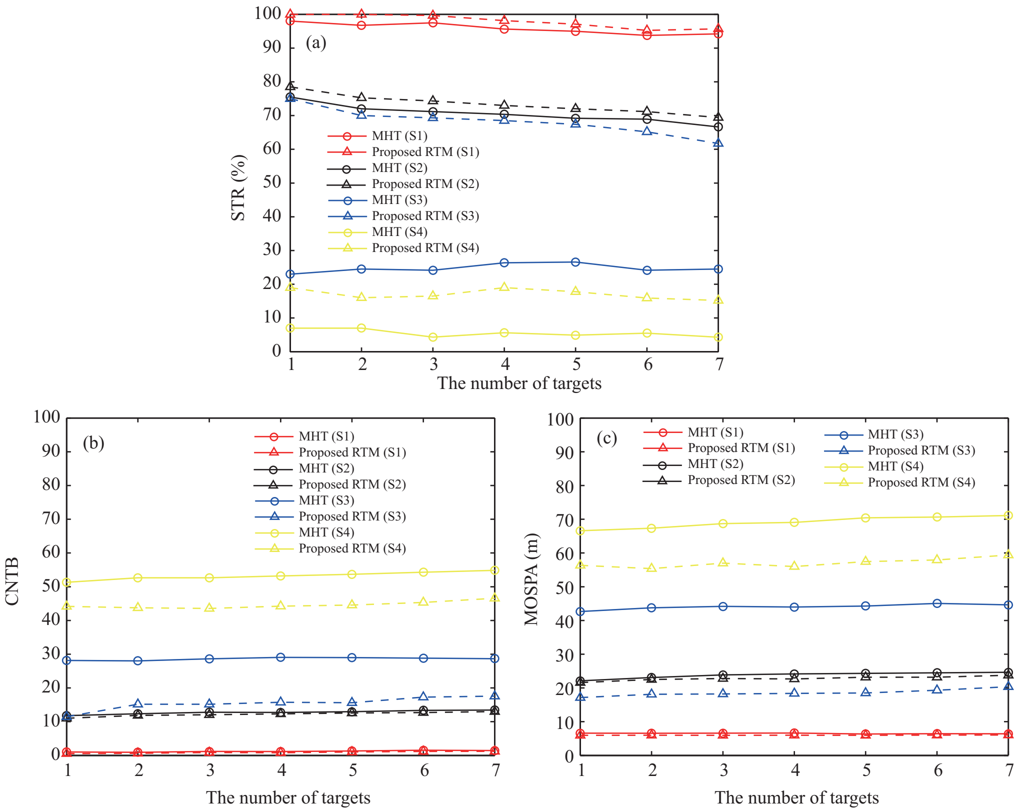

Figure 10 (Color online) Performance comparison of different numbers of targets. (a) STR; (b) CNTB; (c) MOSPA. S1–S4 indicate scenarios 1–4 designed in Table 4.

Table 5 Initial target states

Target index	Kinematic state
1	$[800\ \mathrm{m}, 15\ \mathrm{m/s}, 900\ \mathrm{m}, 15\ \mathrm{m/s}]^{\mathrm{T}}$
2	$[800\ \mathrm{m}, 15\ \mathrm{m/s}, 1100\ \mathrm{m}, 15\ \mathrm{m/s}]^{\mathrm{T}}$
3	$[800\ \mathrm{m}, 15\ \mathrm{m/s}, 2000\ \mathrm{m}, -15\ \mathrm{m/s}]^{\mathrm{T}}$
4	$[800\ \mathrm{m}, 15\ \mathrm{m/s}, 2200\ \mathrm{m}, -15\ \mathrm{m/s}]^{\mathrm{T}}$
5	$[800\ \mathrm{m}, 15\ \mathrm{m/s}, 700\ \mathrm{m}, 15\ \mathrm{m/s}]^{\mathrm{T}}$
6	$[800\ \mathrm{m}, 15\ \mathrm{m/s}, 500\ \mathrm{m}, 15\ \mathrm{m/s}]^{\mathrm{T}}$
7	$[800\ \mathrm{m}, 15\ \mathrm{m/s}, 2400\ \mathrm{m}, -15\ \mathrm{m/s}]^{\mathrm{T}}$

generated seven targets scenario in the case of maneuver index $\lambda = 1$.

Figure 10 shows that for scenarios 1 and 2 with weak fluctuation, compared with MHT, the performance of the proposed RTM is slightly improved. Additionally, the increase in the number of targets has little impact on the tracking performance because of high detection probability under the condition of weak fluctuation. For scenario 3 with strong fluctuation and weak maneuver, the STR of MHT is less than 30%, as shown by the solid blue line in Figure 10(a). However, the performance of the proposed RTM improves significantly. As shown by the blue dotted line in Figure 10(a), the STR can reach 75% with an increase of about 50%. Meanwhile, as the number of targets increases, the performance decreases slightly. Because in multitarget scenarios, when SNR fluctuates strongly, the miss detection probability increases, increasing the false association probability, especially track crossing occurs.

Figure 12 shows the running time comparison with different numbers of targets. Due to poor tracking performance in scenario 4, no comparison is made here. Obviously, as the number of targets increases, the running time increases. However, compared with MHT, the running time of the proposed RTM is only slightly increased. When the number of targets is 7, the difference is at most 1.3 s.

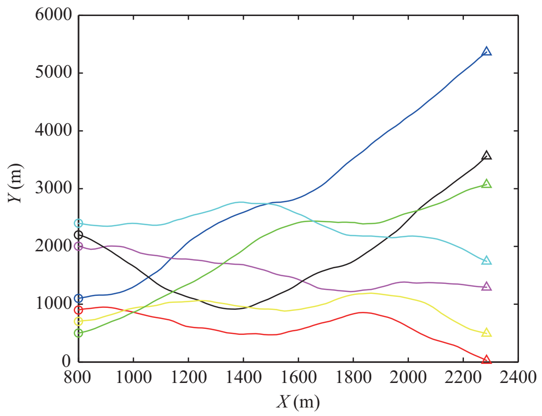

Figure 11 (Color online) Set of target trajectories for $\lambda = 1$ ('o'-start position, '△'-stop position).

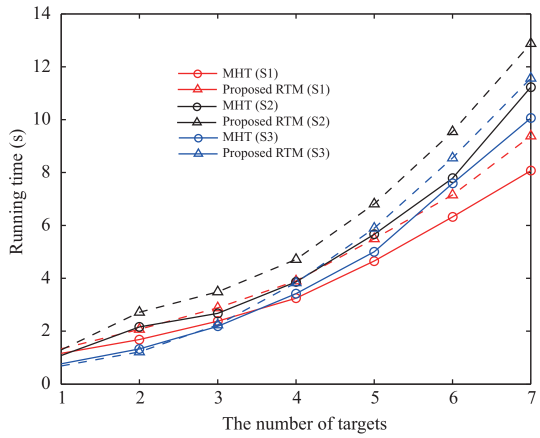

Figure 12 (Color online) Comparison of running time with different numbers of targets.

(a)

(b)

Figure 13 (Color online) (a) Experimental scenarios; (b) bird targets captured by the optical camera (the above and below figures correspond to scenarios 1 and 2 respectively).

4 Experimental data verification

We conducted the observation experiment of bird targets in Dongying City, Shandong Province, China in October 2019. The experimental location, as shown in Figure 13(a), is close to wetlands and lakes. The experimental equipment is a high resolution and fully polarimetric radar working in the Ku band. The main system parameters are shown in Table 6.

We selected two groups of experimental data to evaluate the algorithm's performance. The pictures taken by the optical camera at the same moment are shown in Figure 13(b). Figure 14 shows the tracking result comparisons between the proposed RTM and MHT algorithm. It can be seen that the number of targets is consistent with Figure 13(b), which verifies the correctness of the tracking results. For the proposed RTM, the black dots are the measurements from the constant false alarm detection module, and the blue triangles are the measurements from the measurement set reconstruction module. For the MHT algorithm, once the detection performance declines due to the echo power fluctuation, the measurements at that moment will miss; thereby causing track breakages and increasing the probability of false association. However, for the proposed RTM, if there is a missed detection, the missed measurement will be supplemented by the measurement set reconstruction process based on the feedback track information. Additionally, it also handles maneuvering situations well. Therefore, the proposed method can effectively improve the stability of the bird target tracking.

Table 6 Radar system parameters

Parameter	Value
Carrier centre frequency	16 GHz
Range resolution	0.2 m
Bandwidth	800 MHz
Sample interval	0.1 s
False alarm probability	10^{-6}

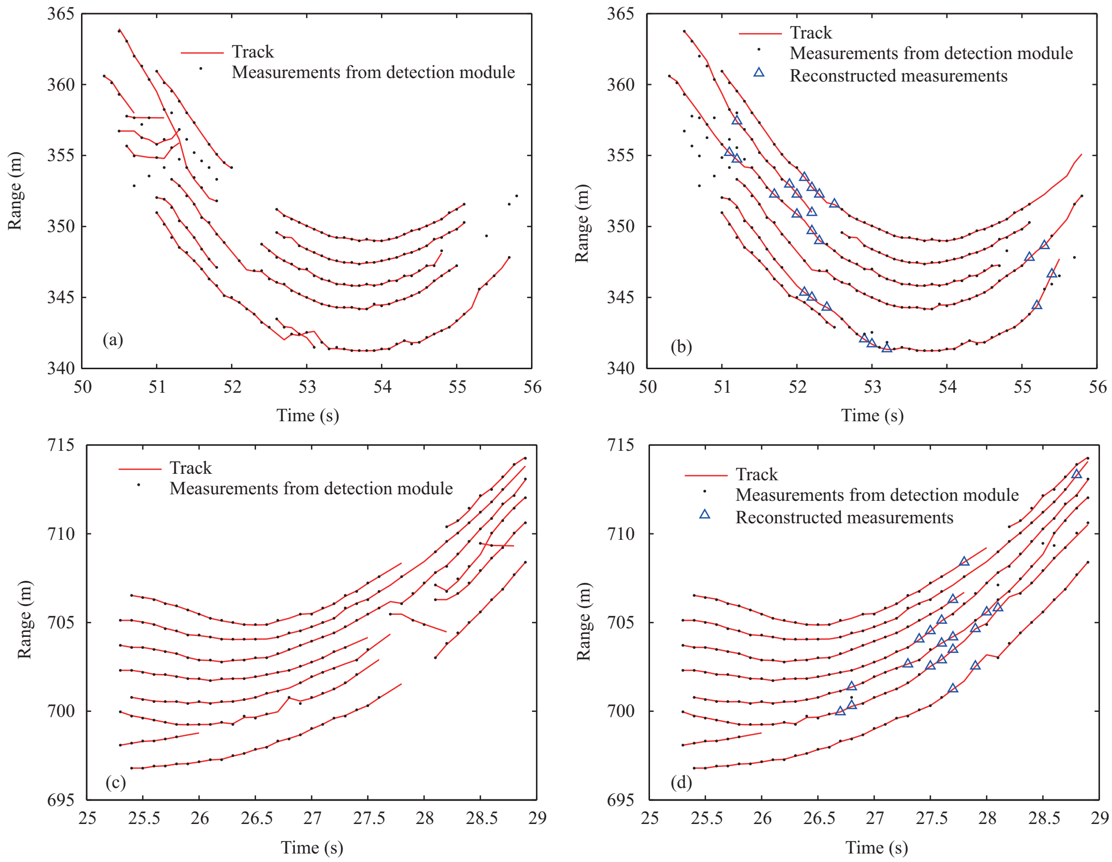

Figure 14 (Color online) Tracking result comparisons of real bird targets. (a) MHT for scenario 1; (b) proposed RTM for scenario 1; (c) MHT for scenario 2; (d) proposed RTM for scenario 2.

5 Conclusion

In this paper, we proposed an RTM that accommodates the echo power fluctuation and maneuver characteristics of bird targets. The design of measurement set reconstruction optimizes the track continuity when the echo power fluctuates. Then, the hypothesis generation and hypothesis probability are modified to improve the data association accuracy. The adaptive parameters filtering strategy has high universality for the flexible maneuvering trajectory. Simulations in scenarios with different SNR levels, different fluctuating and maneuvering levels show significant improvement of the tracking performance. The scenarios with different numbers of targets verify the effectiveness for multitarget tracking and high calculation efficiency. Based on the observation data of bird targets acquired by field experiments, we obtain that the proposed method can effectively reduce the number of track breakages, improve track quality and achieve stable tracking of bird targets.

Acknowledgements This work was supported by National Natural Science Foundation of China (Grant Nos. 31727901, 62001021, 61971037).

References

1 Chen X L, Chen W S, Rao Y H, et al. Progress and prospects of radar target detection and recognition technology for flying birds and unmanned aerial vehicles. J Radar, 2020, 4: 803–827

2 van Doren B M, Horton K G. A continental system for forecasting bird migration. Science, 2018, 361: 1115–1118
3 Cui K, Hu C, Wang R, et al. Deep-learning-based extraction of the animal migration patterns from weather radar images. Sci China Inf Sci, 2020, 63: 140304
4 Nohara T J, Eng B, Eng M, et al. An overview of avian radar developments — past, present and future. In: Proceedings of the 9th Annual Meeting Bird Strike Committee, Kingston, 2007
5 Hu C, Wang Y X, Wang R, et al. An improved radar detection and tracking method for small UAV under clutter environment. Sci China Inf Sci, 2019, 62: 029306
6 Flock W L, Green J L. The detection and identification of birds in flight, using coherent and noncoherent radars. Proc IEEE, 1974, 62: 745–753
7 Li W D, Hu C, Wang R, et al. Comprehensive analysis of polarimetric radar cross-section parameters for insect body width and length estimation. Sci China Inf Sci, 2021, 64: 122302
8 Hu C, Li W Q, Wang R, et al. Insect flight speed estimation analysis based on a full-polarization radar. Sci China Inf Sci, 2018, 61: 109306
9 Beason R C, Nohara T J, Weber P, et al. Beware the boojum: caveats and strengths of avian radar. Hum-Wildl Interact, 2013, 7: 16–46
10 Fortmann T, Bar-Shalom Y, Scheffe M, et al. Detection thresholds for tracking in clutter — a connection between estimation and signal processing. IEEE Trans Autom Control, 1985, 30: 221–229
11 Kershaw D J, Evans R J. A contribution to performance prediction for probabilistic data association tracking filters. IEEE Trans Aerosp Electron Syst, 1996, 32: 1143–1148
12 Aslan M S, Saranlı A, Baykal B. Tracker-aware adaptive detection: an efficient closed-form solution for the Neyman-Pearson case. Digit Signal Process, 2010, 20: 1468–1481
13 Willett P, Niu R, Bar-Shalom Y. Integration of Bayes detection with target tracking. IEEE Trans Signal Process, 2001, 49: 17–29
14 Koch W. Fixed-interval retrodiction approach to Bayesian IMM-MHT for maneuvering multiple targets. IEEE Trans Aerosp Electron Syst, 2000, 36: 2–14
15 Blackman S S. Multiple hypothesis tracking for multiple target tracking. IEEE Aerosp Electron Syst Mag, 2004, 19: 5–18
16 Pasha S A, Vo B N, Tuan H D, et al. A Gaussian mixture PHD filter for jump Markov system models. IEEE Trans Aerosp Electron Syst, 2009, 45: 919–936
17 Dong P, Jing Z L, Gong D R, et al. Maneuvering multi-target tracking based on variable structure multiple model GMCPHD filter. Signal Process, 2017, 141: 158–167
18 Dunne D, Kirubarajan T. Multiple model multi-Bernoulli filters for manoeuvering targets. IEEE Trans Aerosp Electron Syst, 2013, 49: 2679–2692
19 Yi W, Jiang M, Hoseinnezhad R. The multiple model Vo-Vo filter. IEEE Trans Aerosp Electron Syst, 2017, 53: 1045–1054
20 Chen W S, Liu J, Chen X L, et al. Non-cooperative UAV target recognition in low-altitude airspace based on motion model. J Beijing Univ Aeronaut Astronaut, 2019, 45: 687–694
21 Liu J X, Wang Z L, Xu M. DeepMTT: a deep learning maneuvering target-tracking algorithm based on bidirectional LSTM network. Inf Fusion, 2020, 53: 289–304
22 Zhou H. A current statistical model and adaptive tracking algorithm for maneuvering targets. J Guid Control Dyn, 1983, 7: 596–602
23 Cui G L, DeMaio A, Piezzo M. Performance prediction of the incoherent radar detector for correlated generalized Swerling-Chi fluctuating targets. IEEE Trans Aerosp Electron Syst, 2013, 49: 356–368
24 Dowdy P C. RCS probability distribution function modeling of a fluctuating target. In: Proceedings of IEEE Nationa Radar Conference, Los Angeles, 1991. 164–168
25 Gelfand S B, Fortmann T E, Bar-Shalom Y. Adaptive detection threshold optimization for tracking in clutter. IEEE Trans Aerosp Electron Syst, 1996, 32: 514–523
26 Bar-Shalom Y, Blackman S S, Fitzgerald R J. Dimensionless score function for multiple hypothesis tracking. IEEE Trans Aerosp Electron Syst, 2007, 43: 392–400
27 Ba H X, He X Y, Fang Z, et al. A new variance adaptive filtering algorithm for maneuvering target tracking. J Wuhan Univ Technol, 2011, 35: 448–452
28 He Y, Xiu J J, Guan X, et al. Radar Data Processing with Applications. 3rd ed. Beijing: Publishing House of Electronics Industry. 2013
29 Schuhmacher D, Vo B T, Vo B N. A consistent metric for performance evaluation of multi-object filters. IEEE Trans Signal Process, 2008, 56: 3447–3457
30 Kirubarajan T, Bar-Shalom Y. Kalman filter versus IMM estimator: when do we need the latter? IEEE Trans Aerosp Electron Syst, 2003, 39: 1452–1457